Received: 27 May 2021 | Revised: 23 July 2021 | Accepted: 3 August 2021

DOI: 10.1002/ptr.7245

RESEARCH ARTICLE

WILEY

Pseudoephedrine and its derivatives antagonize wild and mutated severe acute respiratory syndrome-CoV-2 viruses through blocking virus invasion and antiinflammatory effect

Shaopeng Yu[1] | Yao Chen[1] | Yusen Xiang[2] | He Lin[3] | Mengge Wang[2] | Wenbo Ye[1] | Pei Zhang[1] | Hongzhuan Chen[2] | Guoqiang Lin[1] | Yuying Zhu[1] | Lili Chen[2] | Jiange Zhang[1]

[1]The Research Center of Chiral Drugs, Innovation Research Institute of Traditional Chinese Medicine (IRI), Shanghai University of Traditional Chinese Medicine, Shanghai, China

[2]Institute of Interdisciplinary Integrative Medicine Research, Shanghai University of Traditional Chinese Medicine, Shanghai, China

[3]The Third Research Institute of Ministry of Public Security, Shanghai, China

Correspondence

Yuying Zhu and Jiange Zhang, The Research Center of Chiral Drugs, Innovation Research Institute of Traditional Chinese Medicine (IRI), Shanghai University of Traditional Chinese Medicine, Shanghai 201203, China.
Email: ying.yu.zhu@163.com (Y. Z.) and jgzhang@shutcm.edu.cn (J. Z.)

Lili Chen, Institute of Interdisciplinary Integrative Medicine Research, Shanghai University of Traditional Chinese Medicine, Shanghai 201203, China.
Email: llchen@shutcm.edu.cn

Funding information

Emergency Scientific Research Programme of Shanghai University of Traditional Chinese Medicine, Grant/Award Numbers: 2019YJ 06-01, 2019YJ 06-03; Scientific Research Project of Shanghai Municipal Health Commission on Traditional Chinese Medicine for Prevention and Treatment of COVID-19, Grant/Award Numbers: 2020XGKY07, 2020XGKY09; Shanghai University of Traditional Chinese Medicine, Grant/Award Numbers: 2019YJ 06-01, 2020XGKY09, 2020XGKY07; The Third Research Institute of Ministry of Public Security; Department of Pharmacy, Nanjing University of Chinese Medicine

The coronavirus disease 2019 has infected over 150 million people worldwide and led to over 3 million deaths. Severe acute respiratory syndrome (SARS)-CoV-2 lineages B.1.1.7, B.1.617, B.1.351, and P.1 were reported to have higher infection rates than that of wild one. These mutations were noticed to happen in the receptor-binding domain of spike protein (S-RBD), especially mutations N501Y, E484Q, E484K, K417N, K417T, and L452R. Currently, there is still no specific medicine against the virus; moreover, cytokine storm is also a dangerous factor for severe infected patients. In this study, potential S-RBD-targeted active monomers from traditional Chinese medicine *Ephedra sinica* Stapf (ephedra) were discovered by virtual screening. NanoBiT assay was performed to confirm blocking activities of the screened compounds against the interaction between SARS-CoV-2 S-RBD and angiotensin-converting enzyme 2 (ACE2). We further analyzed the blocking effect of the active compounds on the interactions of mutated S-RBD and ACE2 by computational studies. Moreover, antiinflammatory activities were evaluated using qRT-PCR, enzyme-linked immune sorbent assay, and Western blot analysis. As a result, pseudoephedrine (MHJ-17) and its derivative (MHJ-11) were found as efficient inhibitors disrupting the interactions between ACE2 and both wild and mutated S-RBDs. In addition, they also have antiinflammatory activities, which can be potential drug candidates or lead compounds for further study.

KEYWORDS

antiinflammatory, ephedrine derivative, SARS-CoV-2, S-RBD mutation

Abbreviations: ACE2, angiotensin-converting enzyme 2; COVID-19, coronavirus disease 2019; DOPE, Discrete Optimised Protein Energy; LPS, Lipopolysaccharide; MTT, 3-(4,5-Dimethyl-2-Thiazolyl)-2,5-Diphenyl Tetrazolium Bromide; PDB, Protein Data Bank; PPI, protein–protein interactions; qRT-PCR, Quantitative Real-time PCR; SARS, severe acute respiratory syndrome; SPR, surface plasmon resonance; S-RBD, receptor-binding domain of spike protein; TCM, traditional Chinese medicine.

Shaopeng Yu, Yao Chen, and Yuseng Xiang contributed equally to this study.

1 | INTRODUCTION

Since late 2019, an epidemic called coronavirus disease 2019 (COVID-19) caused by severe acute respiratory syndrome (SARS)-CoV-2 virus has swept rapidly to the world (Rubin, Baden, Morrissey, & Campion, 2020; Wu, Leung, & Leung, 2020). To date, over 200 countries and regions have invaded by the disease. In addition, over 150 million people worldwide have been infected. Compared with SARS-CoV in 2003, a higher mortality was observed in this disease and led to over 3 million deaths. High infectious capacity was another property in this epidemic (Chu et al., 2020). The world economy was also suffered in a great loss (Ayittey, Ayittey, Chiwero, Kamasah, & Dzuvor, 2020). Moreover, it was reported that inflammatory cytokine storm was also a common symptom in patients with severe COVID-19 and usually led to higher death rate (Abou-Ismaila, Diamonda, Kapoorc, Arafaha, & Nayak, 2020; Scheen, Marre, & Thivolet, 2020). It is worth noting that there is no specific drug yet on the market. However, drug discovery is a lengthy and arduous mission, especially for this kind of RNA viruses such as SARS-CoV-2. Mutations are always occurred during replication, and several kinds of mutant viruses were discovered independently in many countries, such as England, India, South Africa, and Japan (Frampton et al., 2021; Johansen & Nohynek, 2021; Muñoz, Patiño, Ballesteros, Paniz-Mondolfi, & Ramírez, 2021; Oshitani, 2020). In all kinds of mutated viruses, SARS-CoV-2 lineages B.1.1.7, B.1.617, B.1.351, and P.1 are the most notably varieties, because they have higher infectious capacity than that of the wild virus, especially lineage B.1.617 has caused a great disaster in India recently. These lineages of viruses have many mutations in receptor-binding domain (RBD) of S1 subunit of SARS-CoV-2, especially mutations N501Y, E484Q, E484K, L452R, K417N, and K417T (Ostrov, 2021; Verghese et al., 2021). Therefore, although vaccines are available worldwide, multi-target drug for anti-SARS-CoV-2 and antiinflammatory is still desirable. Furthermore, it is still urgent to search for a drug candidate or a lead compound that is effective against both wild and mutated viruses.

Traditional Chinese medicine (TCM) was proved to be advantageous in treating COVID-19, because it has an efficacy and comprehensive therapeutic theory (Li et al., 2020; Liu et al., 2020). Among reported clinically effective treatment schemes of TCM for treating COVID-19 by Zhang and co-workers (Zheng et al., 2020), *Ephedra sinica* Stapf (ephedra) was used for several times. Also, it was also reported that water distillate of ephedra was found to be effective in alleviating the inflammatory and arthritis response (Yeom et al., 2006). As the herb had been reported to be efficacious both on COVID-19 and antiinflammatory, the active components and molecular mechanisms are of great significance, because it may alleviate the trouble caused by both virus invasion and inflammation. In addition, the x-ray structures of lineages B.1.1.7 and B.1.617 receptor-binding domains of spike protein (S-RBDs) and angiotensin-converting enzyme 2 (ACE2) complexes are still unreported. However, they can still be constructed using homology modeling, and mutated S-RBD–ACE2 protein–protein interactions (PPIs) can also be predicated by software. Moreover, as spike protein of lineage B.1.351 (Protein Data Bank [PDB] id = 7LYN) was reported by Gobeil and co-workers (Gobeil et al., 2021), S-RBD of this variety was obtained by intercepting the x-ray structure from amino acid sequence 330–583 (S-RBD part). In addition, an x-ray structure of P.1 variety S-RBD complexed with ACE2 was reported by Dejnirattisai and co-workers (Dejnirattisai et al., 2021), so the crystal structure was used for docking experiment without further simulations. Therefore, compounds against variant viruses can also be screening in silico.

Herein, we investigated active components derived from ephedra and evaluated their blocking activities between S-RBD and ACE2 through virtual screening. We found that ephedrine and pseudoephedrine are potent agents worthy of further study. Then, a NanoBiT assay was performed to evaluate these two compounds and their commercially available derivatives for their inhibitory activities against the interaction between S-RBD and ACE2. Moreover, to confirm whether they can disrupt the interaction between mutated S-RBDs and ACE2, S-RBD models of lineages B.1.1.7 and B.1.617 were constructed by homology modeling, and S-RBD complexed with ACE2 models of lineages B.1.1.7, B.1.617, and B.1.351 was predicted by protein–protein docking. Molecular docking was also used to verify whether these compounds have potent activity to block the interaction between mutated S-RBDs (lineages B.1.1.7, B.1.617, B.1.351, and P.1) and ACE2. For the positive candidates, antiinflammatory activities were also determined to prove that they have potent activities of antiinflammatory cytokine storm, indicating that they are antiviral and antiinflammatory agents. The results revealed that pseudoephedrine (MHJ-17) and its derivative (MHJ-11) are promising and safe inhibitors that could block the interaction between ACE2 and both wild and mutated S-RBDs. In addition, they are also multi-target candidates for their antiinflammatory activities, which could be used as lead compounds for further study.

2 | MATERIALS AND METHODS

2.1 | Compounds

All the ephedrine derivatives were purchased from commercial suppliers or from our laboratory compound library. All these molecules were at least 99.5% purity and were used without any purification. Chemical structures and compound ID of each molecule were shown in Figure 1.

2.2 | Virtual screening and molecular docking

Protein preparation and binding-site definition were performed using protocols inside the program Discovery Studio 4.0 (v 4.0.0.13258). Small molecules were prepared under prepare ligands followed by full minimization protocols. CHARMm forcefield was used in both preparation procedures of proteins and small molecules. All compounds were tried to dock into the crystal structure of S-RBD and ACE2

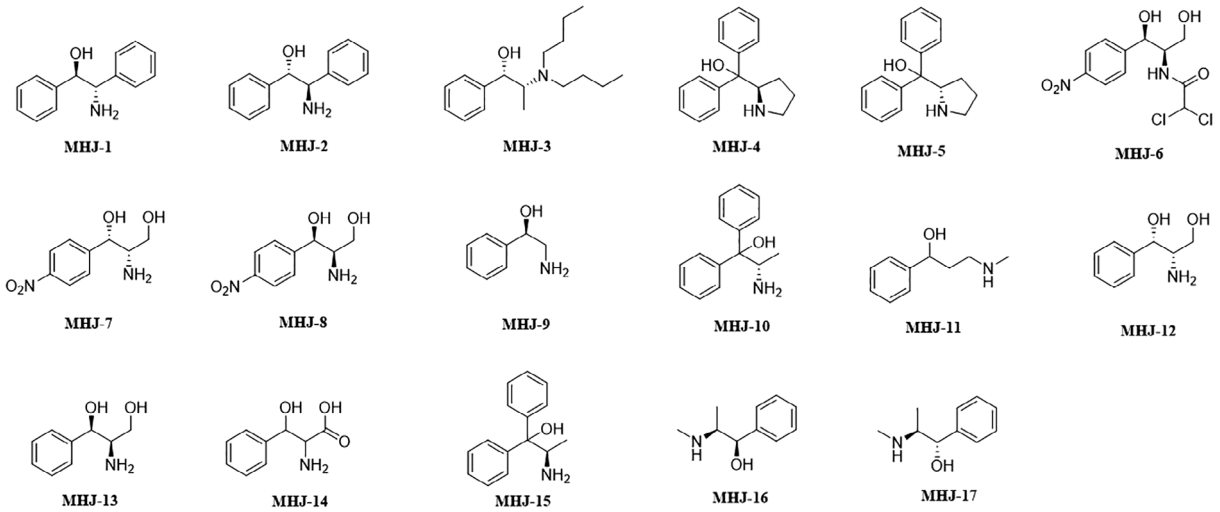

FIGURE 1 Structures of all tested compounds

complex (PDB id = 6M0J) (Lan et al., 2020). Lineage P.1 S-RBD and ACE2 complex (PDB id = 7NXC) were downloaded from PDB and were prepared using Discovery Studio 4.0. Libdock protocol was used in high throughput screening of small molecules with potential activity of disrupting the interaction between wild S-RBD and ACE2. The physical properties and libdock scores were used to conclude active ingredients. CDOCKER protocol was used in molecular docking experiments to judge whether active components could block the interaction between mutated S-RBD and ACE2. A combination of physical properties and scores of CDOCKER ENERGY and CDOCKER INTERACTION ENERGY were used to select the final pose.

2.3 | Sequence alignment and homology modeling

The amino acid sequence of lineages B.1.1.7 and B.1.617 mutated S-RBDs was downloaded from PubMed website (https://www.ncbi.nlm.nih.gov). The S-RBDs of two x-ray structures of S-RBD–ACE2 complex (PDB id = 6M0J and 6ZGG; Lan et al., 2020; Wrobel et al., 2020) were used as templates for homology modeling for their high identity to mutated S-RBDs of SARS-CoV-2 lineages B.1.1.7 and B.1.617. Mutated S-RBD sequences downloaded in the previous step were aligned to the sequences corresponding to wild S-RBD crystal structures using align sequences protocol within the program Discovery Studio 4.0. For building of a protein amino acid sequence into its 3D structure, homology modeling is a more reliable protocol than build mutants procedure (Dubreuil et al., 2005). Thus, build homology models protocol was used to build mutated S-RBD models. The number of models generated was set as 20. Optimization level was set as high, and refine loops were set as true. A combination of probability density function (PDF) total energy, Ramachandran plot, and DOPE score was used to choose the final conformation.

2.4 | Protein–protein docking and conformation refinement

The models of mutated S-RBD built in last step and the crystal structure of the spike protein of lineage B.1.351 (PDB id = 7LYN) downloaded from PDB as well as the ACE2 part of S-RBD–ACE2 complex (PDB id = 6M0J) were prepared and minimized using prepare protein protocol. We made an attempt to find out the strength of interaction of mutated S-RBDs and ACE2, so that their binding mode can be predicated based on their PPIs, which will also give a message about the small-molecule binding site between the two proteins.

ZDOCK protocol was used to perform protein–protein docking between the prepared proteins. The mutated S-RBDs were set as ligands, and the ACE2 was defined as receptor. Angular step size was set as 6°; 2,000 poses were generated for each docking process, and a distance cutoff of 8 Å was used to filter poses. A RMSD cutoff value of 6 Å and an interface cutoff value of 9 Å were used to cluster poses. The ranking of the poses was done, and electrostatic and desolvation energy were calculated during docking processes. The predicated docking conformations calculated by ZDOCK procedure were subjected to refinement and re-ranking using RDOCK protocol to minimize the complexes under CHARMm forcefield. Finally, the final poses were selected from a comprehensive consideration of ZDOCK scores, ZRank scores, and RDOCK scores among all refined conformations.

2.5 | NanoBiT-based SARS-CoV-2 S-RBD/ACE2 binding assay

The preliminary screening and 50% inhibitory concentration (IC_{50}) determination of the 17 compounds (Figure 1) to block SARS-CoV-2 S-RBD/ACE2 interaction were performed by NanoBiT-based assay

according to our previous procedure (Yu et al., 2020). In brief, SARS-CoV-2 S-RBD-LgBiT and SmBiT-ACE2 fusion plasmids were transiently co-transfected into HEK293 cells in a six-well plate using FuGENE HD transfection reagent (Promega, Madison, WI) according to the manufacturer's instructions. After transfection for 6 hr, cells were detached by gentle pipetting, suspended in fresh Opti-MEM medium (Gibco-BRL/Invitrogen, Carlsbad, CA) containing 2% FBS and reseeded into a 96-well plate. To measure if the test compounds could block the interaction between SARS-CoV-2 S-RBD and ACE2, the compounds were serially diluted to indicated concentrations and added to the wells of the 96-well plate and incubated for 3 hr at 37°C. Then, Nano-Glo live Cell Assay reagent was added, and luminescence was measured on an Envision plate reader (EnVision, Perkin Elmer, Waltham, MA). False positive results were considered by determining the cytotoxicity of the compounds on the HEK293 cells and the inhibitory effects of the compounds on NanoLuc (HEK293/Nanoluc stable cells), respectively. Data were analyzed and expressed using the inhibitory effects on SARS-CoV-2 S-RBD/ACE2 interaction (NanoBiT inh%), NanoLuc luciferase (NanoLuc inh%), and the cell proliferation (Cytotox inh%, CC_{50}) on HEK293 cells.

2.6 | Cell viability assays

Raw264.7 cell viability impacted by MHJ-11 or MHJ-17 was detected with MTT method. Cells were treated with different concentrations of MHJ-11 or MHJ-17 for 48 hr; then, MTT solution (0.5 mg/ml) was added to each well. After incubating at 37°C for 5 hr, the formazan crystals in viable cells were dissolved with 100-μL DMSO. Solubilized formazan was spectrophotometrically quantified with Tecan M1000Pro Multiscan Spectrum (Tecan) at 490 nm.

2.7 | qRT-PCR assays

LPS (0.1 μg/ml) was used to activate inflammatory response of RAW264.7 cells. Ctrl group represented normal cells without LPS or drugs treated. Model group represented cells treated with LPS. MHJ-11 groups represented cells treated with LPS and MHJ-11 (125, 250, and 500 μM). MHJ-17 groups represented cells treated with LPS and MHJ-17 (125, 250, and 500 μM). Raw264.7 cells were treated in a 37°C, 5% CO_2 incubator for 6 hr, and total RNA was extracted using TRIzol reagent (Sangon Biotech). Total RNA was then used for reverse transcription with PrimeScript™ RT reagent kit (TaKaRa, Tokyo, Japan), and TB Green™ Premix Ex Taq™ (TaKaRa) was used for qRT-PCR analysis. The mRNA levels were normalized to the β-actin mRNA. Relative quantification was performed as $2^{-\Delta\Delta Ct}$. Three repeats were executed for each assay. Amplification primers were as follows: IL-6 (F: 5′-CTGCA AGAGA CTTCC ATCCA G-3′, R: 5′-AGTGG TATAG ACAGG TCTGT TGG-3′), TNF-α (F:5′-CTGTA GCCCA CGTCG TAGC-3′, R: 5′-TTGAG ATCCA TGCCG TTG-3′), and β-actin (F: 5′-GTCCC TCACC CTCCC AAAAG-3′, R: 5′-GCTGC CTCAA CACCT CAACC C-3′).

2.8 | Enzyme-linked immune sorbent assays

Ctrl, Model, MHJ-11, and MHJ-17 groups were set as those in qRT-PCR analysis. Raw264.7 cells were treated for 24 hr, and the supernatants were collected for IL-6 and TNF-α detection. Protein levels were measured by enzyme-linked immune sorbent assay (ELISA) according to the manufacturer's instructions (NeoBioscience, Shanghai, China). Three repeats were executed for each assay.

2.9 | Western blot

Ctrl and Model groups were set as those in qRT-PCR analysis. MHJ-11 group represented cells treated with LPS and 500-μM MHJ-11. MHJ-17 group represented cells treated with LPS and 500-μM MHJ-17. Raw264.7 cells were treated for 24 hr; then, cells were collected and lysed with NP40 buffer (Beyotime Biotechnology, Shanghai, China) according to manufacturer's instructions. Western blots were performed as described using antibodies against phospho-NFκB p65 (Cell Signaling Technology, 3,033), phospho-p44/42 MAPK (Cell Signaling Technology, 4,376), phospho-SAPK/JNK (Cell Signaling Technology, 4,668), phospho-p38 (Cell Signaling Technology, 4,511), phospho-IκBα (Cell Signaling Technology, 2,859), and β-actin (Cell Signaling Technology, 3,700; Zhu et al., 2020). Detections were analyzed with Azure Biosystem (Azure c600, Azure Biosystem™, Dublin, CA). Three repeats were executed for each assay.

2.10 | Data analysis

The raw data were analyzed using GraphPad Prism 8.0.1 software. Two-tailed Student's *t* test was used to determine the significance of differences in the above-mentioned assays. All values are presented as mean ± SD. The *P* value was used to indicate statistical significance.

3 | RESULTS

3.1 | Virtual screening

The aim of our virtual screening was to search for active ingredients derived from TCM *Ephedra sinica* Stapf (ephedra), which could block the interaction between S-RBD of SARS-CoV-2 and ACE2. Therefore, a crystal structure of S-RBD and ACE2 complex (PDB id = 6M0J) was used as docking target. The long and narrow binding site was detected from receptor cavities by the function within Discovery Studio 4.0. Among the candidates successfully docked into the cavity, we found that ephedrine (MHJ-16) and pseudoephedrine (MHJ-17) were the most potent ingredients in disrupting the interaction between SARS-CoV-2 S-RBD and ACE2, and their CDOCKER interaction energies were lower than other candidates. Therefore, it could be predicted that ephedrine, pseudoephedrine, or their derivatives may have

potent activity in blocking the interaction. The binding site of the crystal structure and docking pose of ephedrine were shown in Figure 2.

3.2 | Blocking activities of three compounds on the SARS-CoV-2 S-RBD/ACE2 interaction

The inhibitory activities of ephedrine (MHJ-16), pseudoephedrine (MHJ-17), and 15 corresponding commercial derivatives against SARS-CoV-2 S-RBD/ACE2 interaction were investigated by NanoBiT assay. Fortunately, three compounds (MHJ-11, MHJ-16, and MHJ-17) were active according to preliminary screening results. Then, these three active compounds were further verified in a dose-dependent manner. As shown in Figure 3, the IC_{50} values of these three compounds on S-RBD/ACE2 interaction (NanoBiT inh%), NanoLuc luciferase (NanoLuc inh%), and HEK293 cells proliferation (Cytotox inh%) were analyzed. Notably, none of the three compounds showed obvious inhibitory effects on Nanoluc luciferase (IC_{50} > 100 μM), and they had low cytotoxicity to HEK293 cells (IC_{50} > 100 μM; Figure 3). Among the three compounds, MHJ-17 (IC_{50} = 13 μM) showed better blocking activity compared with MHJ-11 (IC_{50} = 49 μM) and MHJ-16 (IC_{50} = 73 μM). Therefore, these three compounds showed blocking activity against the interaction between SARS-CoV-2 S-RBD and ACE2, although MHJ-16 exhibited lower activity.

3.3 | Homology modeling and protein–protein docking

Homology modeling is a powerful and widely used tool to build and predict 3D structures of proteins whose folded forms are unknown (Waterhouse et al., 2018). Although x-ray structure of lineage B.1.1.7 S-RBD complexed with antibody was reported (Supasa et al., 2021), the structure of the protein docked with natural receptor may be quite different. To reveal a more accurate result, homology modeling was used in this research. Two different S-RBD parts of x-ray structures of S-RBD–ACE2 complex (PDB id = 6M0J and 6ZGG) were used as templates. Both templates were combined with their endogenous receptor protein ACE2. SARS-CoV-2 lineage B.1.1.7 has a mutation called N501Y, and lineage B.1.617 is used to refer to two mutations in S protein at the positions E484Q and L452R. These varieties caused the infection rates of these viruses increased dramatically. Fortunately, the sequences of mutated viruses can be downloaded from PubMed website. As shown in Figure 4, sequence alignment revealed that these sequences are highly homologous, and mutations N501Y, E484Q, and L452R were highlighted in red. In the building procedure of S-RBD of lineage B.1.1.7, 20 molecular models were generated during initial procedure, and the best model (Figure 5a,b) with the lowest PDFs total energy and PDF physical energy of 8,820.1 and 591.4, respectively, was chosen for further CHARMm forcefield refinement and research. In another hand, S-RBD of lineage B.1.617 was built under the same procedure, and the PDF total energy and PDF physical energy of the best model were 9,075.5 and 764.0, respectively. Ramachandran plots of the two generated models were also shown in Figure 5c,d, and it was indicated that most of the amino acids in the best predicated model were considered favorable. Importantly, the highlighted mutated residues N501Y of B.1.1.7, and E484Q and L452R of B.1.617 were also in green, indicating that the built models are reliable.

ZDOCK and RDOCK protocols were used to generate and refine protein–protein docking complex, respectively. As the crystal structure of spike protein of lineage B.1.351 (PDB id = 7LYN) was reported (Gobeil et al., 2021), the RBD part of it was directly used at this stage. As a result, eight poses for variety B.1.1.7, 12 poses for variety B.1.617, and 28 poses for variety B.1.351 complexed with ACE2 were generated, which were further refined and re-ranked using CHARMm forcefield. The best docking pose of each procedure was selected under a consideration of highest ZDOCK score and lowest E_RDOCK, which was considered as the conformation closest to the real. The best pose of lineage B.1.1.7 S-RBD–ACE2 complex was shown in Figure 6, and the contacting surface area was observed like the previous wild S-RBD–ACE2 complex. However, in the constructed model, the interacting amino acid residues of both parts are different from the previous one (Table 1 and Figure 6b,c,e,f,h,i). It was visualized that Arg403, Asn439, Tyr473, Gly476, Glu484, Cys488, Phe490, Pro499, Val503, and Gln506 in lineage B.1.1.7 S-RBD were interacted with ACE2 protein, which did not occur before. Residues Lys417 and Gly446 in the new model had no interaction with ACE2. Moreover, it could be observed that Ser19, Thr324, Gln325, Gly326, Glu329, Gly352, Phe356, and Ala386 were interacted with lineage B.1.1.7 S-RBD, which were not detected before. Also, Glu35, Glu37, Gln42, Arg357, and Arg393 were not interacted with mutated S-RBD as

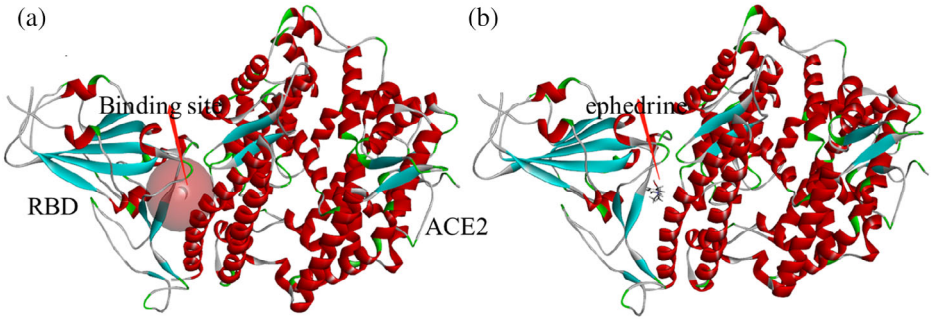

FIGURE 2 (a) The binding site of receptor-binding domain of spike protein–angiotensin-converting enzyme 2 complex. (b) Ephedrine docked into the cavity successfully

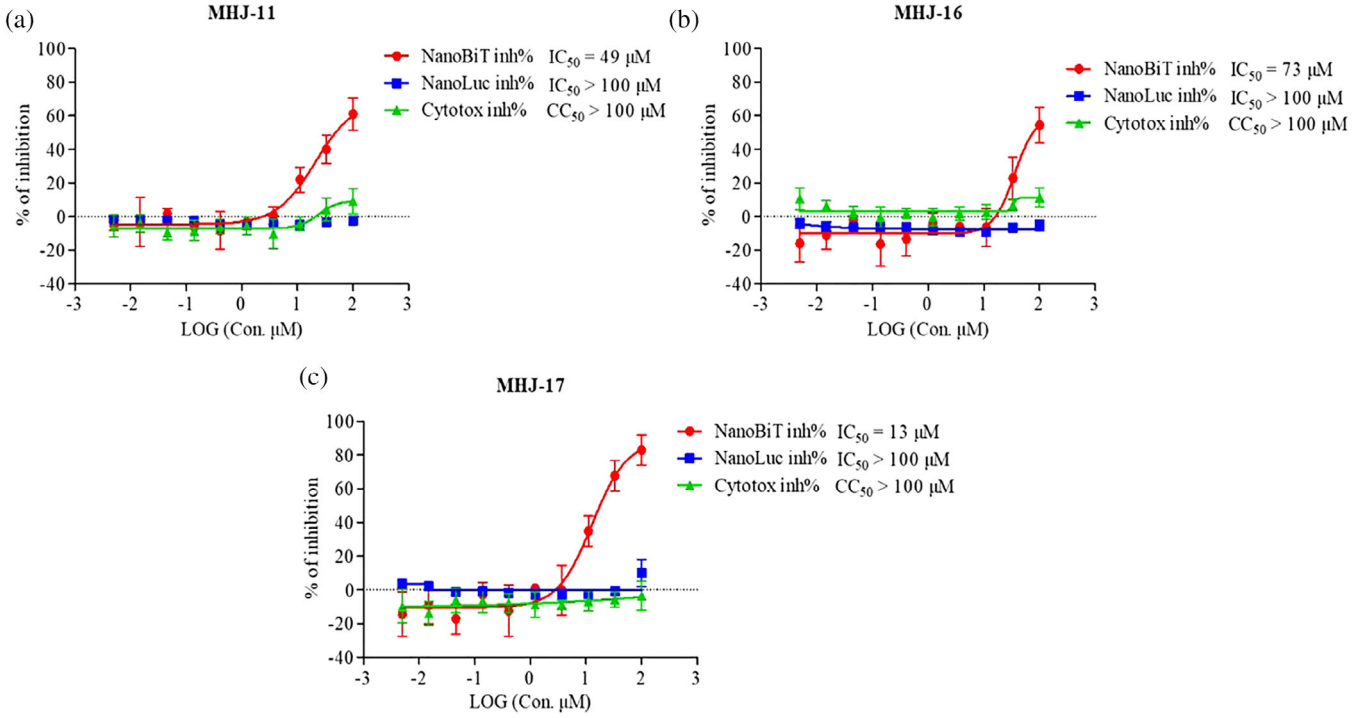

FIGURE 3 NanoBiT-based severe acute respiratory syndrome (SARS)-CoV-2 receptor-binding domain of spike protein (S-RBD)/angiotensin-converting enzyme 2 (ACE2) interaction assay for MHJ-11, MHJ-16, and MHJ-17. NanoBiT inh%: the inhibition rates against SARS-CoV-2 S-RBD/ACE2 interaction; NanoLuc inh%: the inhibition rates against NanoLuc luciferase; Cytotox inh%: the inhibition rates against the transfected HEK293 cells proliferation. $n = 3$

FIGURE 4 The sequences of two templates and mutated receptor-binding domains of spike protein

these interactions were collected using x-ray structures of wild S-RBD–ACE2 complex. On the other hand, S-RBD of B.1.617 variety complexed with ACE2 indicated that Arg403, Asn439, Tyr473, Gly476, Ser477, Gln484, and Pro499 were new interacted amino acid residues with ACE2. Furthermore, Ser19, Glu23, Thr324, Gln325, Gly326, Phe356, and Ala386 in ACE2 were interacted with S-RBD of B.1.617 variety, which has never happened before. At last, analysis of S-RBD of lineage B.1.351 complexed with ACE2 indicated that Arg403, Asp405, Lys458, Tyr473, Gln474, Gly476, Ser477, Lys484, Ser494, and Pro499 from S-RBD have new interactions with ACE2. Also, Ser19, Thr20, Glu23, Lys26, Thr324, Gln325, Gly326, Phe327, Phe356, Met383, Ala384, Ala386, and Ala387 were observed to have interactions with ACE2. As a result, all the mutated S-RBDs and ACE2 had more amino acid residues interact with each other. It may be explained that mutated viruses resulted in higher transmissibility than the previous viruses (Chan et al., 2020).

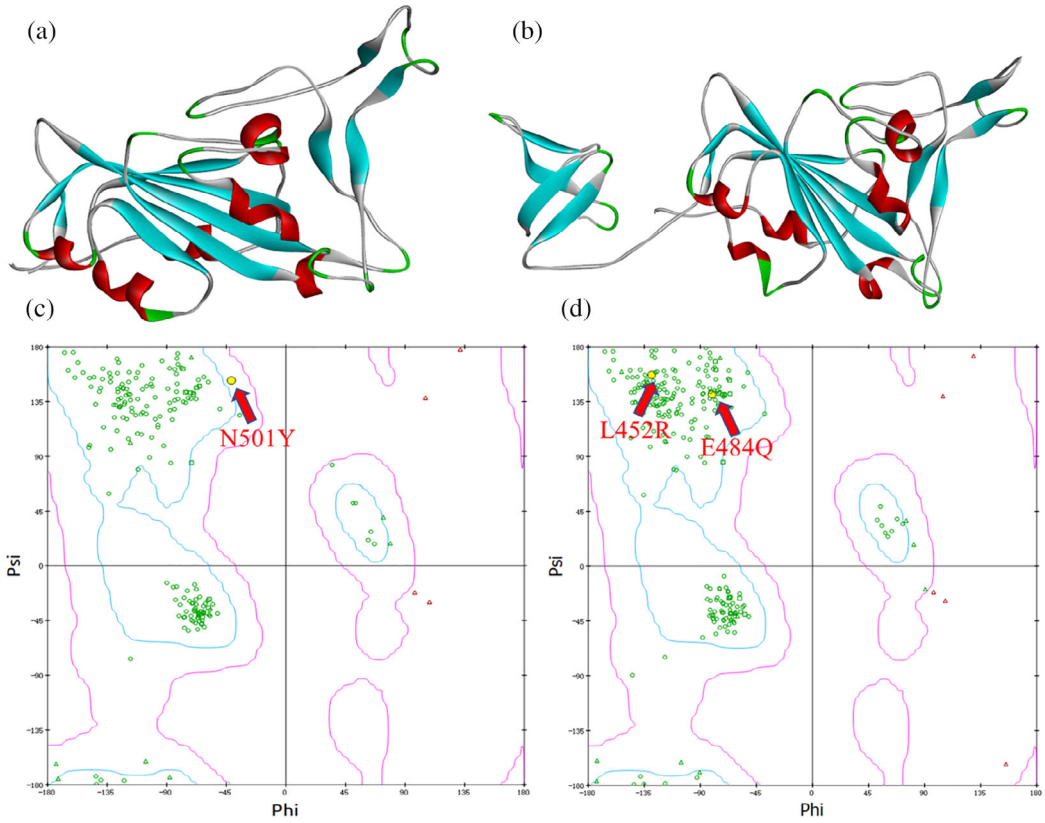

FIGURE 5 (a) Constructed receptor-binding domain of spike protein (S-RBD) model of severe acute respiratory syndrome (SARS)-CoV-2 lineage B.1.1.7. (b) Constructed S-RBD model of SARS-CoV-2 lineage B.1.617. (c) Ramachandran plot of the lineage B.1.1.7 S-RBD protein. (d) Ramachandran plot of lineage B.1.617 S-RBD protein

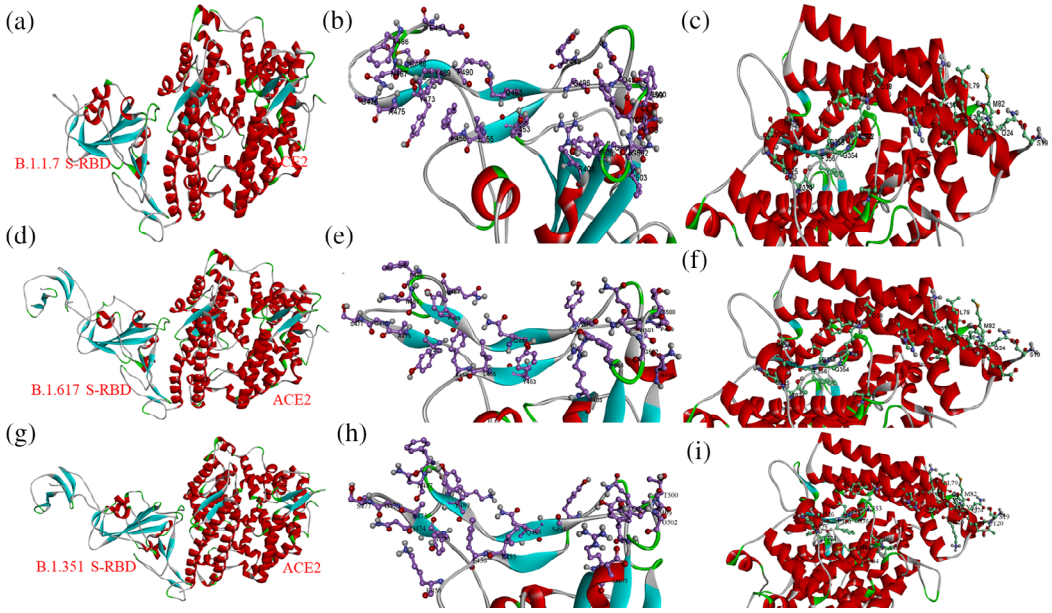

FIGURE 6 (a) Lineage B.1.1.7 receptor-binding domain of spike protein (S-RBD) interacts with angiotensin-converting enzyme 2 (ACE2). (b,c) Interacting amino acid residues of lineage B.1.1.7 S-RBD and ACE2. (d) Lineage B.1.617 S-RBD interacts with ACE2. (e,f) Interacting amino acid residues of lineage B.1.617 S-RBD and ACE2. (g) Lineage B.1.351 S-RBD interacts with ACE2. (h,i) Interacting amino acid residues of lineage B.1.351 S-RBD and ACE2

TABLE 1 Interacting amino acid residues between angiotensin-converting enzyme 2 and wild and mutated receptor-binding domains of spike protein

Wild RBD	B.1.1.7 RBD	B.1.617 RBD	B.1.351 RBD	ACE2 with wild RBD	ACE2 with B.1.1.7 RBD	ACE2 with B.1.617 RBD	ACE2 with B.1.351 RBD
	Arg403	Arg403	Arg403		Ser19	Ser19	Ser19
			Asp405				Thr20
Lys417						Glu23	Glu23
	Asn439	Asn439		Gln24	Gln24	Gln24	Gln24
							Lys26
Gly446				Thr27	Thr27	Thr27	Thr27
Tyr449	Tyr449	Tyr449	Tyr449	Phe28	Phe28	Phe28	Phe28
Tyr453	Tyr453	Tyr453		Asp30	Asp30	Asp30	Asp30
Leu455	Leu455	Leu455	Leu455	Lys31	Lys31	Lys31	Lys31
Phe456	Phe456	Phe456	Phe456	His34	His34	His34	His34
			Lys458	Glu35			
	Tyr473	Tyr473	Tyr473	Glu37			
			Gln474	Asp38	Asp38	Asp38	
Ala475	Ala475	Ala475	Ala475	Tyr41	Tyr41	Tyr41	Tyr41
	Gly476	Gly476	Gly476	Gln42			
		Ser477	Ser477	Leu79	Leu79	Leu79	Leu79
	Glu484	Gln484	Lys484	Met82	Met82	Met82	Met82
Phe486	Phe486	Phe486	Phe486	Tyr83	Tyr83	Tyr83	Tyr83
Asn487	Asn487	Asn487	Asn487		Thr324	Thr324	Thr324
	Cys488				Gln325	Gln325	Gln325
Tyr489	Tyr489	Tyr489	Tyr489		Gly326	Gly326	Gly326
	Phe490						Phe327
Gln493	Gln493	Gln493	Gln493		Glu329		
			Ser494	Asn330	Asn330	Asn330	
Gly496	Gly496	Gly496			Gly352		
Gln498	Gln498	Gln498	Gln498	Lys353	Lys353	Lys353	Lys353
	Pro499	Pro499	Pro499	Gly354	Gly354	Gly354	Gly354
Thr500	Thr500	Thr500	Thr500	Asp355	Asp355	Asp355	Asp355
Asn501	Tyr501	Asn501	Tyr501		Phe356	Phe356	Phe356
Gly502	Gly502	Gly502	Gly502	Arg357			
	Val503						Met383
Tyr505	Tyr505	Tyr505	Tyr505				Ala384
					Ala386	Ala386	Ala386
							Ala387
	Gln506			Arg393			

3.4 | Molecular docking

After explaining the reasons for increased infectious capacity of the new viruses, it was urgent to evaluate whether pseudoephedrine (MHJ-17) and its derivative (MHJ-11) can block the interaction between mutated viruses and ACE2 protein. Molecular docking experiment using CDOCKER protocol within Discovery Studio 4.0 software was performed to solve this problem. It is hard to define binding sites between simulated mutated S-RBDs and ACE2, because the interactions between them are stronger than that of the wild one. Fortunately, both molecules (MHJ-11 and MHJ-17) could dock into the narrow cavities, indicating that these two compounds could also disrupt the interaction between mutated S-RBDs and ACE2. These results showed a prospect of two compounds. In the S-RBD of B.1.1.7 variety and ACE2 complex model, as shown in Figure 7a, MHJ-11 has several π relevant interactions with Gln388, Lys417, and Pro389 and has many strong hydrogen bond interactions with surrounding residues, such as Ala386, Ala387, Gln388, Asp405, and Tyr505. These

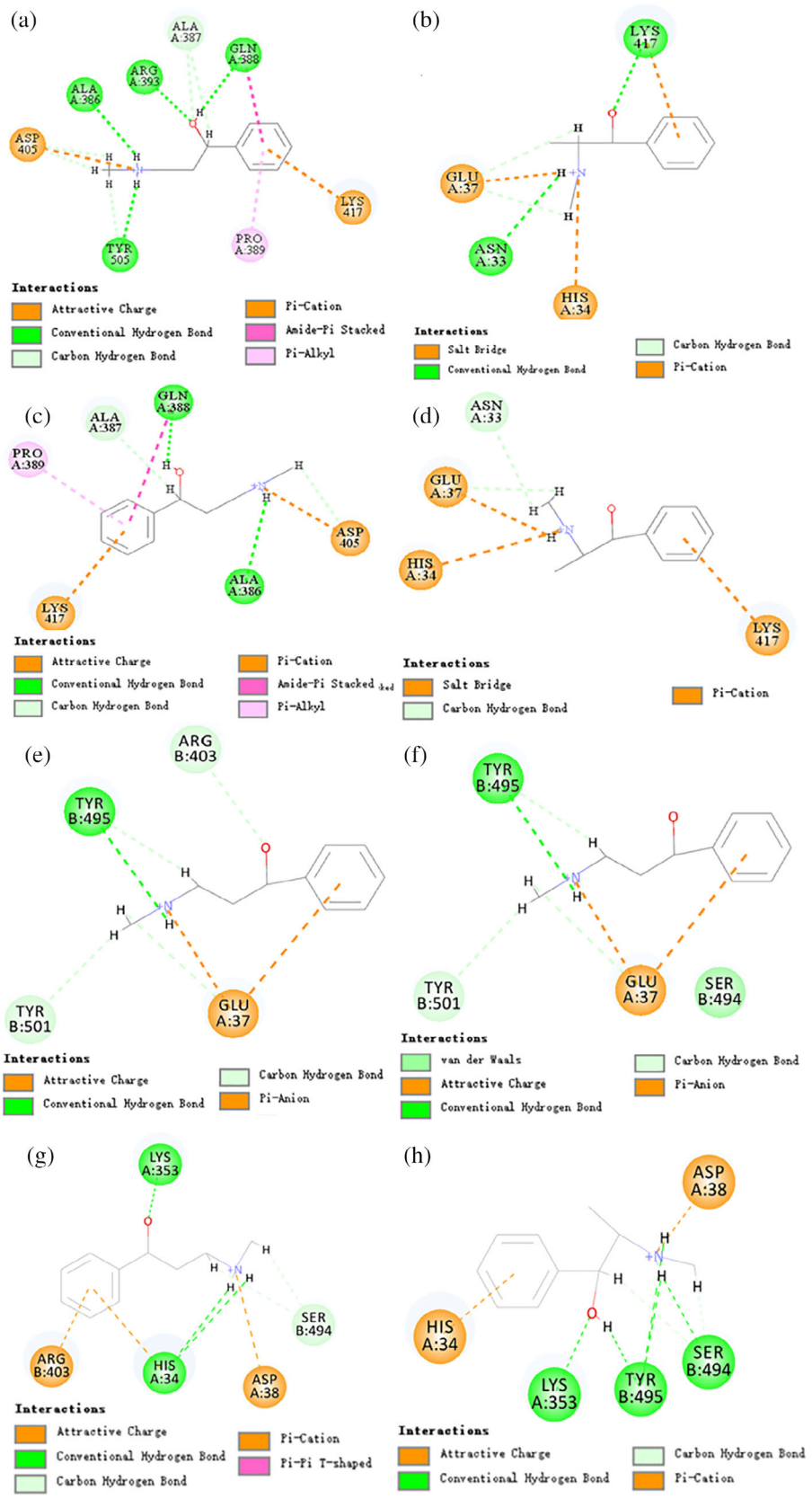

FIGURE 7 (a) Interaction between MHJ-11 and B.1.1.7 receptor-binding domain of spike protein (S-RBD)–angiotensin-converting enzyme 2 (ACE2) complex. (b) Interaction between MHJ-17 and B.1.1.7 S-RBD–ACE2 complex. (c) Interaction between MHJ-11 and B.1.617 S-RBD–ACE2 complex. (d) Interaction between MHJ-17 and B.1.617 S-RBD–ACE2 complex. (e) Interaction between MHJ-11 and lineage B.1.351 S-RBD–ACE2 complex. (f) Interaction between MHJ-17 and lineage B.1.351 S-RBD–ACE2 complex. (g) Interaction between MHJ-11 and lineage P.1 S-RBD–ACE2 complex. (h) Interaction between MHJ-17 and lineage P.1 S-RBD–ACE2 complex

amino acid residues are dispersed across the lineage B.1.1.7 S-RBD and ACE2. Moreover, MHJ-17 can also dock into the complex (Figure 7b). The amino group of MHJ-17 has a salt bridge with His34 and Glu37, and the compound also has several hydrogen bond interactions with Asn33 and Lys417. In addition, the interaction between lineage B.1.617 complexed with ACE2 could also be disrupted by

MHJ-11 and MHJ-17 according to the results by molecular docking. As shown in Figure 7c, MHJ-11 performed π relevant interactions with Gln388, Pro389, and Lys417. Also, the compound has several hydrogen bond and salt bridge interactions with Ala387, Gln388, Ala386, and Asp405. Furthermore, MHJ-17 can form salt bridge interactions with the complex (Figure 7d). Also, it could be observed that the compound has two hydrogen bonds with Asn33 and Glu37. Under the same strategy, docking experiments were also performed to verify the two compounds on blocking activities for disrupting the interaction between ACE2 and S-RBDs of lineage B.1.351 and P.1. As a result, both MHJ-11 and MHJ-17 could dock into the complexes. As shown in Figure 7e,f, both MHJ-11 and MHJ-17 have several hydrogen bond interactions with the complexes, and they also have π-anion interactions with Glu37. In another hand, both active compounds have many strong hydrogen bond interactions with variety P.1 S-RBD and ACE2 complex (Figure 7g,h) and have π-cation interactions with surrounding amino acid residues. Moreover, according to CDOCKER interaction energy scores calculated in docking experiments, both MHJ-11 and MHJ-17 have stronger interactions with mutated S-RBDs complexed with ACE2 than that of the wild one. In addition, mutated amino acid residues such as N501Y, E484Q, L452R, K417N, and E484K seldom perform interactions with the two active compounds (only mutated amino acid Tyr501 of variety B.1.351 has interactions with MHJ-11 and MHJ-17, Figure 7e,f). Therefore, the mutations did not cause a decrease in activity in blocking PPIs between mutated S-RBDs and ACE2, and MHJ-11 and MHJ-17 can be used as reliable lead compounds for further modification.

3.5 | Antiinflammation activities

As systemic inflammatory response is a major symptom for coronavirus infections, macrophages play critical role in this process. Therefore, we detected the antiinflammation activity of MHJ-11 and MHJ-17 in Raw264.7 cells. As shown in Figure 8, the cytotoxicity of MHJ-11 (Figure 8a) and MHJ-17 (Figure 8b) was not observed in Raw264.7 cells until the concentration reached 400 μM. After that, the expression and transcriptional levels of two representative inflammatory factors, IL-6 and TNF-α, were measured after treatment with different concentrations of MHJ-11 and MHJ-17. The results showed that MHJ-11 could significantly reduce the mRNA and protein levels of IL-6 at 125, 250, and 500 μM in LPS-activated Raw264.7 cells (Figure 8c,d). Similarly, MHJ-17 could also greatly downregulate IL-6 mRNA and protein expression of at 125, 250, and 500 μM in LPS-activated Raw264.7 cells (Figure 8c,d). Furthermore, MHJ-11 could significantly reduce the mRNA and protein levels of TNF-α at 500 μM (Figure 8e,f), and MHJ-17 could significantly reduce TNF-α mRNA and protein expression at 250 and 500 μM (Figure 8e,f). Thus, the antiinflammation effects were observed for MHJ-11 and MHJ-17.

We then explored the inflammation-related pathways regulated by MHJ-11 and MHJ-17. Phosphorylation of NFκB p65, p44/42 MAPK, SAPK/JNK, p38, and IκBα proteins was detected by Western blot with LPS-activated Raw264.7 cells treated with 500-μM MHJ-11 or MHJ-17. As shown in Figure 9, MHJ-11 and MHJ-17 could significantly inhibit protein phosphorylation of NFκB p65 (Figure 9b), p44/42 MAPK (Figure 9c), SAPK/JNK (Figure 9d), p38 (Figure 9e), and IκBα (Figure 9f), which indicated that the two active compounds could regulate NFκB and MAPK signaling pathway to inhibit inflammatory response.

4 | DISCUSSION

COVID-19 has been spreading for over 1 year and may continue for a long time (Daughton, 2020; Ouslander & Grabowski, 2020). This kind of novel virus can spread during the asymptomatic period or form asymptomatic persons, and the number of infected people is larger than 150 million and is still increasing. Moreover, it is worth noting that patients infected with this virus are usually accompanied by an inflammatory factor storm that could make the death rate dramatically increased. Therefore, attention should be paid to antiinflammation while treating COVID-19 (Zhang et al., 2020). Furthermore, with the evolution of this virus, several lineages have determined as more dangerous mutated forms with high infection and low detection rates (Li et al., 2020; Dorpa et al., 2020), such as lineage B.1.1.7 first found in England, B.1.617 first found in India, B.1.351 first found in South Africa, and P.1 first found in Brazil. Recently, a mutation called D614G is relevant to virus transmissibility enhancement and also opens a potential binding pocket at the interface of spike protein (Ostrov, 2021). Because amino acid D614 is not located in S-RBD and may not affect S-RBD/ACE2 interaction, it is not investigated in this study. Several reports have indicated that these mutations were occurred in the S-RBDs and may allow the viruses to undergo immune escape to existing vaccines (Saghazadeh & Rezaei, 2020; Pinto et al., 2020). Thus, searching for a broad-spectrum PPI inhibitor with antiinflammatory activity is an urgent and long-term task.

Ephedra, the traditional Chinese herb medicine, was reported to have both activities in treating COVID-19 clinically and in antiinflammatory effect in vivo (Li, Li, et al., 2020; Liu et al., 2020), which is very attractive to us. Initially, we performed virtual screening to judge whether ingredients from ephedra could have activities of blocking the interaction between SARS-CoV-2 S-RBD and ACE2 protein. As the two parts of the protein complex were combined tightly with each other, the binding site defined by Discovery Studio 4.0 software was narrow. This means that small and long molecules have advantages in docking into the cavity, while bulky compounds hardly show activities in this docking model. The virtual screening results showed that small molecules, ephedrine and pseudoephedrine, may have the activity for disrupting the PPI between SARS-CoV-2 S-RBD and ACE2.

With the docking results in hand, next, to further explore whether these two compounds discovered by virtual screening could block the interaction between SARS-CoV-2 S-RBD and ACE2, we performed the NanoBiT assay to determine their inhibitory activities. Meanwhile, as many ephedrine derivatives are commercially available, another 15 compounds were also evaluated in this work. The structures of all

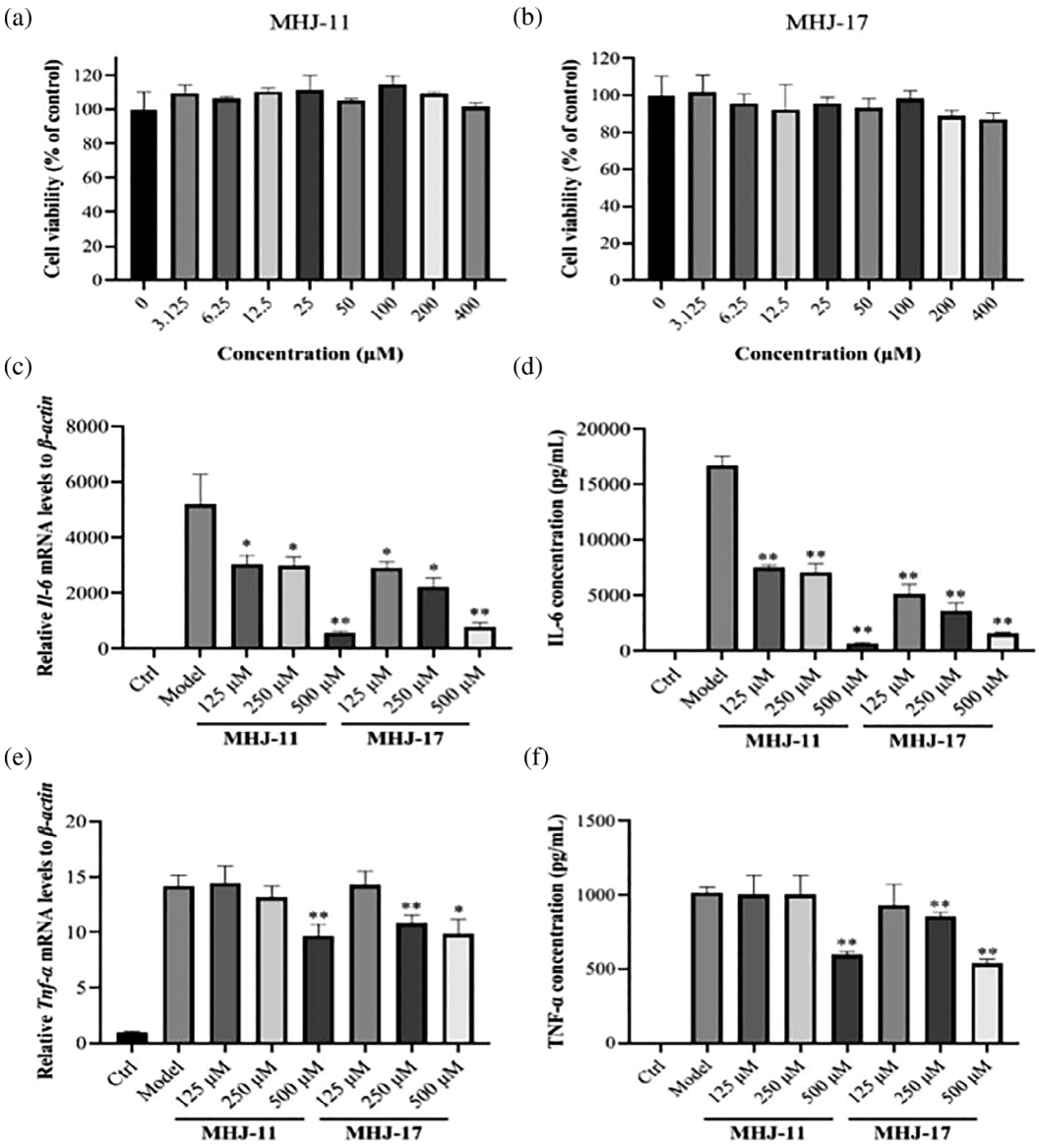

FIGURE 8 Inhibition effects of MHJ-11 and MHJ-17 to inflammatory factors in Raw264.7 cells. (a,b) Cell toxicity of MHJ-11 and MHJ-17 to Raw264.7 cells. (c) Inhibition effect of MHJ-11 and MHJ-17 to IL-6 mRNA levels in Raw264.7 cells. (d) Inhibition effect of MHJ-11 and MHJ-17 to IL-6 protein released by Raw264.7 cells. (e) Inhibition effect of MHJ-11 and MHJ-17 to TNF-α mRNA levels in Raw264.7 cells. (f) Inhibition effect of MHJ-11 and MHJ-17 to TNF-α protein released by Raw264.7 cells. Ctrl group represents normal cells without LPS or drugs treated. Model group represents activated Raw264.7 cells with LPS. $^{*}p < .05$; $^{**}p < .01$. $n = 3$

the tested compounds were shown in Figure 1. The results showed that MHJ-11, MHJ-16, and MHJ-17 had potential activities for inhibiting the interaction. Especially, pseudoephedrine (MHJ-17) exhibited better activity than MHJ-11, and the activity of MHJ-17 was about six times that of ephedrine (MHJ-16). Interestingly, there is only a difference of chiral center between ephedrine and pseudoephedrine, but their activities are quite different. To explain this, we performed the computational docking study. As shown in Figure 10, it can be observed that ephedrine (MHJ-16) has more interactions with S-RBD–ACE2 complex than pseudoephedrine (MHJ-17). However, an unfavorable donor–donor interaction was detected during docking procedure. As reported by Han and co-workers (Lv et al., 2021), ephedrine, pseudoephedrine, and methylephedrine could block SARS-CoV-2 invasion into cells in pseudovirus experiments. They pointed out that the molecular mechanism was that these three compounds could interact with S-RBD and ACE2, respectively, according to surface plasmon resonance assay results. Similarly, in this work, our NanoBiT assay results further explained ephedrine (MHJ-16), and pseudoephedrine (MHJ-17) could inhibit SARS-CoV-2 pseudovirus entry into cells by blocking SARS-CoV-2/ACE2 interaction, and a new derivative MHJ-11 was also reported.

In addition, we further explored how the two PPI inhibitors (MHJ-11 and MHJ-17) could disrupt the interaction between mutated S-RBD and ACE2 protein. Computational studies of homology

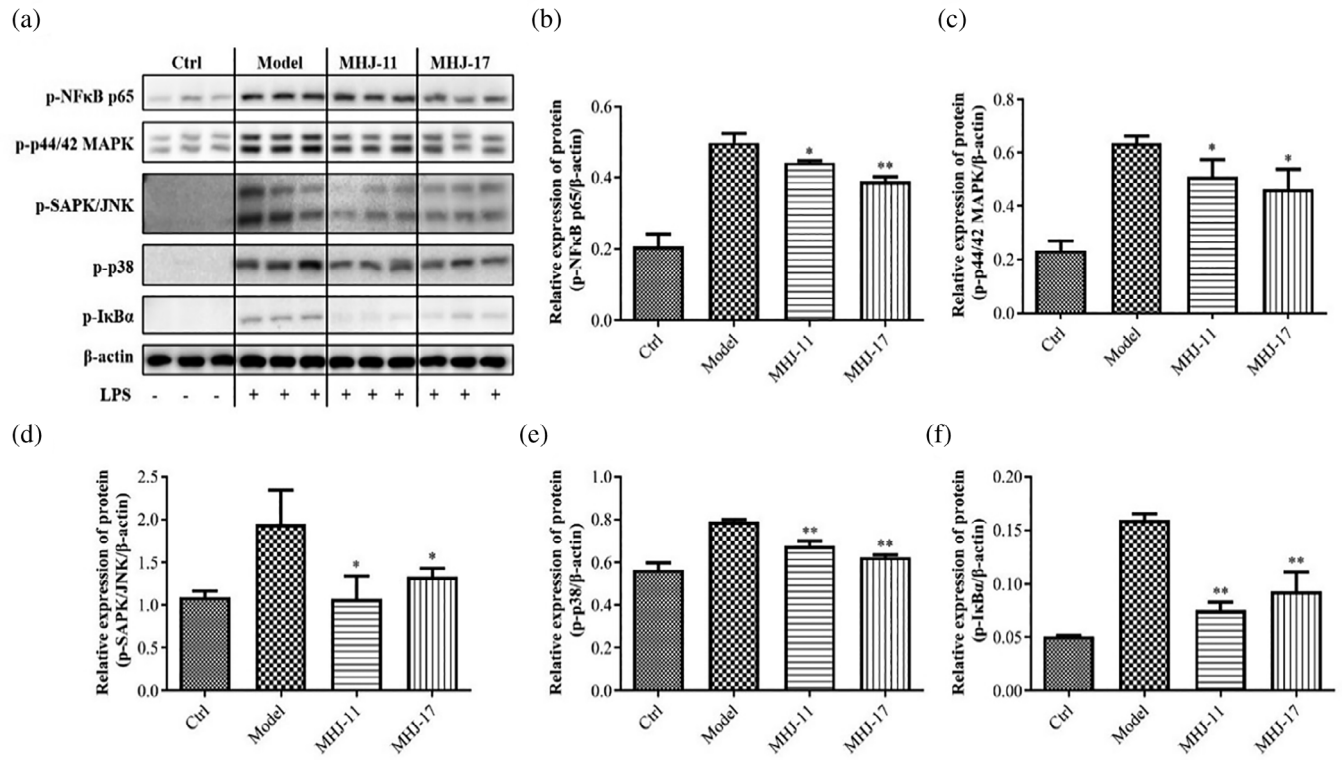

FIGURE 9 Regulation effect of MHJ-11 and MHJ-17 to inflammation-related pathway in Raw264.7 cells. (a) Inflammation-related protein levels impacted by MHJ-11 and MHJ-17 detected with western blot. (b–f) Protein quantification of p-NFκB p65, p-p44/42 MAPK, p-SAPK/JNK, p-p38, and p-IκBα, respectively. Ctrl group represents normal cells without LPS or drugs treated. Model group represents activated Raw264.7 cells with LPS. Concentration of MHJ-11 and MHJ-17 was 500 μM. $^{*}p < .05$; $^{**}p < .01$. $n = 3$

modeling, protein–protein docking, and molecular docking were performed to predict the activity. Although x-ray structure of lineage B.1.1.7 S-RBD and antibody complex had been reported, we still used homology modeling protocol to build the variant S-RBD. This was because poses of proteins complexed with an antibody may be very different to the poses docked to natural receptors. To improve experiment quality, we used the sequences downloaded from PubMed to construct the S-RBD models of a B.1.1.7 variant and a B.1.617 variant, respectively. Two S-RBD parts of wild S-RBD–ACE2 complexes were both used as templates, because sequences of these two S-RBDs are different, and lead to two different structures. The final poses were chosen according to composite scores of PDF total energies, PDF physical energies, and DOPE scores. Then, a B.1.1.7 mutated S-RBD–ACE2 complex model and a B.1.617 variety S-RBD–ACE2 complex model were built. Protein–protein docking, pose refinement, and minimization procedures within Discovery Studio 4.0 were used in sequence. The open S-RBD of B.1.351 variety was intercepted from the x-ray structure of spike protein of the mutated virus (PDB id = 7LYN). As a result, under optimized conditions, eight poses for B.1.1.7 variety S-RBD and ACE2 complex, 12 poses for B.1.617 variety S-RBD and ACE2 complex, and 28 poses for B.1.351 variety S-RBD and ACE2 complex were persisted in 54,000 poses from each simulation procedure. The best pose was chosen according to ZDock scores, ZRand scores, and E-Rdock. Moreover, it could be discovered that two parts of the new complexes were combined tighter than before due to more amino acid residue interactions observed. The built complexes of mutated S-RBDs interact with ACE2 were then used to evaluate whether MHJ-11 and MHJ-17 could also block their PPIs. As two parts of the new models are closer, the binding sites were even smaller than the previous complex. Fortunately, when MHJ-11 and MHJ-17 tried to dock into the narrow binding sites, good results were still feedback, suggesting that these two molecules could also disrupt the interaction between ACE2 and S-RBDs of lineages B.1.1.7, B.1.617, B.1.351, and P.1. These results revealed that both MHJ-11 and MHJ-17 are reliable drug candidates or lead compounds for blocking the interactions between ACE2 and both wild and mutated S-RBDs, which could be used for further research or modification.

Immune response in severe COVID-19 is characterized by cytokine storm, which is associated with untoward clinicopathological consequences (Mahmudpour, Roozbeh, Keshavarz, Farrokhi, & Nabipour, 2020). Studies showed that higher levels of inflammatory factors, including IL-6 and TNF-α, were found in deceased patients of SARS-CoV-2 infection compared with those recovered from the disease (Mehta et al., 2020; Huang et al., 2020). Thus, we also detected the antiinflammatory effect of MHJ-11 and MHJ-17, which inhibited the mRNA and protein levels of IL-6 and TNF-α in LPS-activated Raw264.7 cells. Moreover, the phosphorylation levels of inflammation-related proteins NFκB p65, p44/42 MAPK, SAPK/JNK, p38, and IκBα were all reduced. Therefore, MHJ-11 and MHJ-17 might be multi-target inhibitors against SARS-CoV-2 infections.

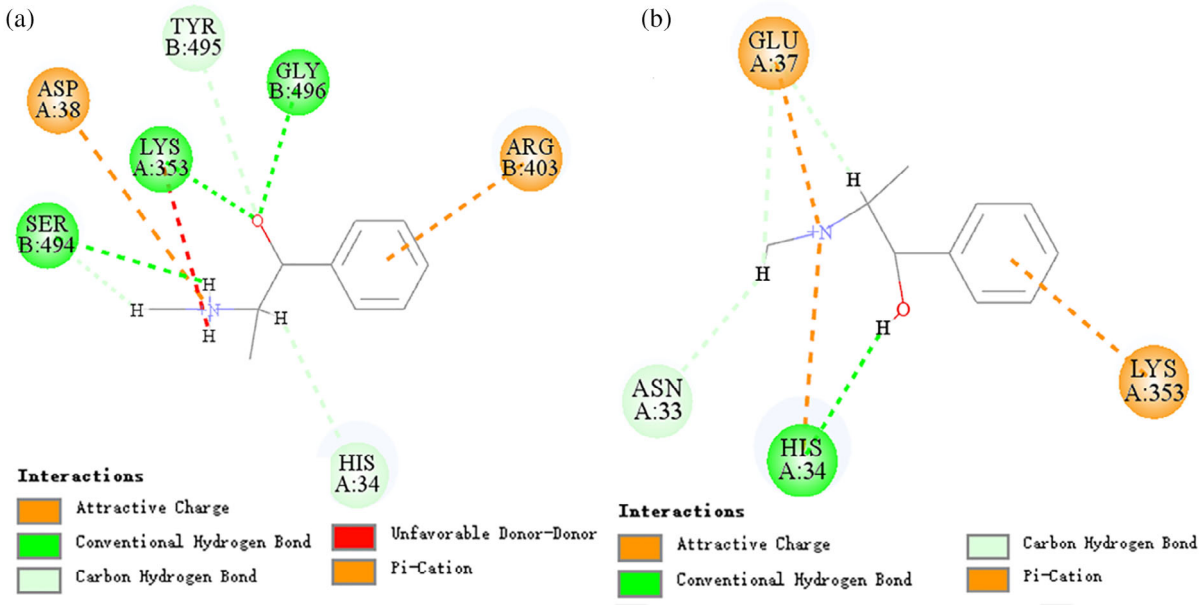

FIGURE 10 (a) Details of ephedrine docked into receptor-binding domain of spike protein (S-RBD)–angiotensin-converting enzyme 2 (ACE2) complex. (b) Details of pseudoephedrine docked into S-RBD–ACE2 complex

5 | CONCLUSIONS

In summary, we have reported two active molecules as SARS-CoV-2 S-RBD–ACE2 PPI inhibitors. Further antiinflammatory experiments indicated that MHJ-11 and MHJ-17 have potent activities of antiinflammatory cytokine storm, which could be considered as potent antiviral and antiinflammatory inhibitors against SARS-CoV-2. Moreover, computer-aided experiments were used to predicate that these two compounds could also block the interaction between S-RBDs of lineages B.1.1.7, B.1.617, B.1.351, and P.1 and ACE2. These results are of great interest to us and will guide us to move on for further research.

ACKNOWLEDGEMENTS

The authors thank Department of Pharmacy, Nanjing University of Chinese Medicine for providing Discovery Studio 4.0. They also thank The Third Research Institute of Ministry of Public Security for providing ephedrine and pseudoephedrine. This work was supported by Scientific Research Project of Shanghai Municipal Health Commission on Traditional Chinese Medicine for Prevention and Treatment of COVID-19 (2020XGKY07; 2020XGKY09) and Emergency Scientific Research Programme of Shanghai University of Traditional Chinese Medicine (2019YJ 06-01; 2019YJ 06-03).

AUTHOR CONTRIBUTIONS

Jiange Zhang, Guoqiang Lin, Lili Chen, and Hongzhuan Chen conceived and supervised the whole study. Shaopeng Yu and Wenbo Ye performed virtual screening, homology modeling, protein–protein docking, and molecular docking. Yuying Zhu, Yao Chen, Yuseng Xiang, and Mengge Wang carried out the experiments and data analysis. Shaopeng Yu, Yuying Zhu, and Lili Chen drafted the manuscript. He Lin, Wenbo Ye, and Pei Zhang contributed to experimental consumables. Jiange Zhang, Guoqiang Lin, Lili Chen, and Hongzhuan Chen revised the manuscript. All data were generated in-house, and no paper mill was used. All authors agree to be accountable for all aspects of work ensuring integrity and accuracy.

CONFLICTS OF INTEREST

The authors declare no competing interests.

DATA AVAILABILITY STATEMENT

The data that support the findings of this study are available from the corresponding author upon reasonable request.

ORCID

Jiange Zhang https://orcid.org/0000-0002-1434-6040

REFERENCES

Abou-Ismaila, M. Y., Diamonda, A., Kapoorc, S., Arafaha, Y., & Nayak, L. (2020). The hypercoagulable state in COVID-19: Incidence, pathophysiology, and management. *Thrombosis Research*, *194*, 101–115.

Ayittey, F. K., Ayittey, M. K., Chiwero, N. B., Kamasah, J. S., & Dzuvor, C. (2020). Economic impacts of Wuhan 2019-nCoV on China and the world. *Journal of Medical Virology*, *92*, 473–475.

Chan, J. F., Zhang, A. J., Yuan, S., Poon, V. K., Chris, C. C., Lee, A. C., … Yuen, K. (2020). Simulation of the clinical and pathological manifestations of coronavirus disease 2019 (COVID-19) in a Golden Syrian hamster model: Implications for disease pathogenesis and transmissibility. *Clinical Infectious Diseases*, *71*, 2428–2446.

Chu, H., Chan, J. F., Wang, Y., Yuen, T. T., Chai, Y., Hou, Y., … Yuen, K. (2020). Comparative replication and immune activation profiles of SARS-CoV-2 and SARS-CoV in human lungs: An ex vivo study with implications for the pathogenesis of COVID-19. *Clinical Infectious Diseases*, *71*, 1400–1409.

Daughton, C. G. (2020). Wastewater surveillance for population-wide Covid-19: The present and future. *Science of the Total Environment*, *736*, 139631.

Dejnirattisai, W., Zhou, D., Supasa, P., Liu, C., Mentzer, A. J., Ginn, H. M., … Screaton, G. R. (2021). Antibody evasion by the P.1 strain of SARS-CoV-2. *Cell*, *184*, 2939–2954.

Dorpa, L., Acmana, M., Richard, D., Shaw, L. P., Ford, C. E., Ormond, L., … Balloux, F. (2020). Emergence of genomic diversity and recurrent mutations in SARS-CoV-2. *Infection, Genetics and Evolution*, *83*, 104351.

Dubreuil, O., Bossus, M., Graille, M., Bilous, M., Savatier, A., Jolivet, M., … Ducancel, F. (2005). Fine tuning of the specificity of an anti-progesterone antibody by first and second sphere residue engineering. *Journal of Biological Chemistry*, *280*, 24880–24887.

Frampton, D., Rampling, T., Cross, A., Bailey, H., Heaney, J., Byott, M., … Nastouli, E. (2021). Genomic characteristics and clinical effect of the emergent SARS-CoV-2 B.1.1.7 lineage in London, UK: A whole-genome sequencing and hospital-based cohort study. *The Lancet Infectious Diseases*. https://www.sciencedirect.com/science/article/pii/S1473309921001705

Gobeil, S. M., Janowska, K., McDowell, S., Mansouri, K., Parks, R., Stalls, V., …, Acharya, P. (2021). Effect of natural mutations of SARS-CoV-2 on spike structure, conformation and antigenicity. bioRxiv, 2021.03.11.435037.

Huang, C., Wang, Y., Li, X., Ren, L., Zhao, J., Hu, Y., … Cao, B. (2020). Clinical features of patients infected with 2019 novel coronavirus in Wuhan, China. *The Lancet*, *395*, 497–506.

Johansen, K., & Nohynek, H. (2021). No country or continent is on its own in the ongoing COVID-19 pandemic. *Eurosurveillance*, *26*, 2100430. https://doi.org/10.2807/1560-7917.ES.2021.26.17.2100430

Lan, J., Ge, J., Yu, J., Shan, S., Zhou, H., Fan, S., … Wang, X. (2020). Structure of the SARS-CoV-2 spike receptor-binding domain bound to the ACE2 receptor. *Nature*, *581*, 215–220.

Li, Q., Wu, J., Nie, J., Zhang, L., Hao, H., Liu, S., … Wang, Y. (2020). The impact of mutations in SARS-CoV-2 spike on viral infectivity and antigenicity. *Cell*, *182*, 1284–1294.

Li, Y., Li, J., Zhong, D., Zhang, Y., Zhang, Y., Guo, Y., … Jin, R. (2020). Clinical practice guidelines and experts' consensuses of traditional Chinese herbal medicine for novel coronavirus (COVID-19): Protocol of a systematic review. *Systematic Reviews*, *9*, 170.

Liu, M., Gao, Y., Yuan, Y., Yang, K., Shi, S., Zhang, J., & Tian, J. (2020). Efficacy and safety of integrated traditional Chinese and Western medicine for Corona virus disease 2019 (COVID-19): A systematic review and meta-analysis. *Pharmacological Research*, *158*, 104896.

Lv, Y., Wang, S., Liang, P., Wang, Y., Zhang, X., Jia, Q., … He, L. (2021). Screening and evaluation of anti-SARS-CoV-2 components from Ephedra sinica by ACE2/CMC-HPLC-IT-TOF-MS approach. *Analytical and Bioanalytical Chemistry*, *413*, 2995–3004.

Mahmudpour, M., Roozbeh, J., Keshavarz, M., Farrokhi, S., & Nabipour, I. (2020). COVID-19 cytokine storm: The anger of inflammation. *Cytokine*, *133*, 155151.

Mehta, P., McAuley, D. F., Brown, M., Sanchez, E., Tattersall, R. S., & Manson, J. J. (2020). COVID-19: Consider cytokine storm syndromes and immunosuppression. *The Lancet*, *395*, 1033–1034.

Muñoz, M., Patiño, L. H., Ballesteros, N., Paniz-Mondolfi, A., & Ramírez, J. D. (2021). Characterizing SARS-CoV-2 genome diversity circulating in south American countries: Signatures of potentially emergent lineages? *International Journal of Infectious Diseases*, *105*, 329–332.

Oshitani, H. (2020). Cluster-based approach to coronavirus disease 2019 (COVID-19) response in Japan, from February to April 2020. *Japanese Journal of Infectious Diseases*, *73*, 491–493.

Ostrov, D. A. (2021). Structural consequences of variation in SARS-CoV-2 B.1.1.7. *Journal of Cellular Immunology*, *3*, 103–108.

Ouslander, J. G., & Grabowski, D. C. (2020). COVID-19 in nursing homes: Calming the perfect storm. *Journal of the American Geriatrics Society*, *68*, 2153–2162.

Pinto, D., Park, Y., Beltramello, M., Walls, A. C., Tortorici, M. A., Bianchi, S., … Corti, D. (2020). Cross-neutralization of SARS-CoV-2 by a human monoclonal SARS-CoV antibody. *Nature*, *583*, 290–295.

Rubin, E. J., Baden, L. R., Morrissey, S., & Campion, E. W. (2020). Medical journals and the 2019-nCoV outbreak. *The New England Journal of Medicine*, *382*, 866.

Saghazadeh, A., & Rezaei, N. (2020). Towards treatment planning of COVID-19: Rationale and hypothesis for the use of multiple immunosuppressive agents: Anti-antibodies, immunoglobulins, and corticosteroids. *International Immunopharmacology*, *84*, 106560.

Scheen, A. J., Marre, M., & Thivolet, C. (2020). Prognostic factors in patients with diabetes hospitalized for COVID-19: Findings from the CORONADO study and other recent reports. *Diabetes & Metabolism*, *46*, 265–271.

Supasa, P., Zhou, D., Dejnirattisai, W., Liu, C., Mentzer, A. J., Ginn, H. M., … Screaton, G. R. (2021). Reduced neutralization of SARS-CoV-2 B.1.1.7 variant by convalescent and vaccine sera. *Cell*, *184*, 2201–2211.

Verghese, M., Jiang, B., Iwai, N., Mar, M., Sahoo, M. K., Yamamoto, F., … Pinsky, B. A. (2021). A SARS-CoV-2 variant with L452R and E484Q neutralization resistance mutations. *Journal of Clinical Microbiology*, *59*, e0074121. https://doi.org/10.1128/JCM.00741-21

Waterhouse, A., Bertoni, M., Bienert, S., Studer, G., Tauriello, G., Gumienny, R., … Schwede, T. (2018). SWISS-MODEL: Homology modelling of protein structures and complexes. *Nucleic Acids Research*, *46*, W296–W303.

Wrobel, A. G., Benton, D. J., Xu, P., Roustan, C., Martin, S. R., Rosenthal, P. B., … Gamblin, S. J. (2020). SARS-CoV-2 and bat RaTG13 spike glycoprotein structures inform on virus evolution and furin-cleavage effects. *Nature Structural & Molecular Biology*, *27*, 763–767.

Wu, J. T., Leung, K., & Leung, G. M. (2020). Nowcasting and forecasting the potential domestic and international spread of the 2019-nCoV outbreak originating in Wuhan, China: A modelling study. *The Lancet*, *395*, 689–697.

Yeom, M., Lee, H., Kim, G., Lee, H., Shim, I., Oh, S., … Hahm, D. (2006). Anti-arthritic effects of Ephedra sinica STAPF herb-acupuncture: Inhibition of lipopolysaccharide-induced inflammation and adjuvant-induced polyarthritis. *Journal of Pharmacological Sciences*, *100*, 41–50.

Yu, S., Zhu, Y., Xu, J., Yao, G., Zhang, P., Wang, M., … Zhang, J. (2020). Glycyrrhizic acid exerts inhibitory activity against the spike protein of SARS-CoV-2. *Phytomedicine*, *85*, 153364. https://doi.org/10.1016/j.phymed.2020.153364

Zhang, W., Zhao, Y., Zhang, F., Wang, Q., Li, T., Liu, Z., … Zhang, S. (2020). The use of anti-inflammatory drugs in the treatment of people with severe coronavirus disease 2019 (COVID-19): The perspectives of clinical immunologists from China. *Clinical Immunology*, *214*, 108393.

Zheng, W., Zhang, J., Yang, F., Wang, Y., Liu, Q., & Zhang, B. (2020). Comprehensive analysis of diagnosis and treatment schemes for prevention and treatment of novel coronavirus pneumonia by traditional Chinese medicine. *Journal of Traditional Chinese Medicine*, *61*, 277–280.

Zhu, Y., Yang, L., Xu, J., Yang, X., Luan, P., Cui, Q., … Zhang, J. (2020). Discovery of the anti-angiogenesis effect of eltrombopag in breast cancer through targeting of HuR protein. *Acta Pharmaceutica Sinica B*, *10*, 1414–1425.

How to cite this article: Yu, S., Chen, Y., Xiang, Y., Lin, H., Wang, M., Ye, W., Zhang, P., Chen, H., Lin, G., Zhu, Y., Chen, L., & Zhang, J. (2021). Pseudoephedrine and its derivatives antagonize wild and mutated severe acute respiratory syndrome-CoV-2 viruses through blocking virus invasion and antiinflammatory effect. *Phytotherapy Research*, *35*(10), 5847–5860. https://doi.org/10.1002/ptr.7245